Electronic Structure and Photocatalytic Characterization of a Novel Photocatalyst $AgAlO_2$

Shuxin Ouyang,[‡,⊥] Haitao Zhang,[‡,⊥] Dunfang Li,[‡,⊥] Tao Yu,[§,⊥] Jinhua Ye,[†] and Zhigang Zou*[,‡,⊥]

Department of Materials Science and Engineering, Nanjing University, Nanjing 210093, P.R. China, Ecomaterials and Renewable Energy Research Center (ERERC), Department of Physics, Nanjing University, Nanjing 210093, P.R. China, National Laboratory of Solid State Microstructures, Nanjing University, Nanjing 210093, P.R. China, and Ecomaterials Center, National Institute for Materials Science, 1-2-1 Sengen, Tsukuba, Ibaraki 305-0047, Japan

Received: October 16, 2005; In Final Form: January 16, 2006

A novel photocatalyst, $AgAlO_2$, was prepared by cation exchange reaction and characterized by powder X-ray diffraction. The result showed $AgAlO_2$ crystallizes in the layered orthorhombic structure with space group was $Pna2_1$. The energy band and electronic structures of $AgAlO_2$ were calculated based on the crystal structure. It was found that $AgAlO_2$ is an indirect band gap semiconductor. The valence band top mainly consists of O-2p orbitals and Ag-4d orbitals and the conduction band bottom is mainly constructed of Ag-5s5p orbitals. The band gap of $AgAlO_2$ was estimated to be about 2.8(1) eV with UV−vis diffuse reflectance spectrometry. The photocatalytic activity of $AgAlO_2$ was characterized by photocatalytically decomposing the dye alizarin red (AR) under visible light irradiation, and AR could be decomposed about 70% under 2 h of visible light irradiation.

I. Introduction

Since Fujishima et al.'s discovery of the photocatalytic property of TiO_2 three decades ago,[1] many studies have been carried out to develop novel semiconductor photocatalysts that are able to split water into H_2 and O_2 with high efficiency. Because electrons in these photocatalysts are excited from the O-2p orbital to transition metal-d orbitals, their band gaps are usually wider, exceeding 3.0 eV.[2] This means that most of these photocatalysts can only exhibit photocatalytic activity under UV irradiation. The ultraviolet light accounts for merely about 4% of the whole solar energy, but the visible light accounts for 43% of the whole solar energy and also the main portion of the indoor artificial illumination. To develop photocatalysts with high activity under visible light, many investigations have been carried out on new materials with a narrow band gap. Anion doping of the transition metal oxides, such as $TiO_{2-x}N_x$,[2] TaON,[3−6] etc., could decrease the band gap. Though the light absorption was increased to visible, the defects introduced by doping would accelerate recombination of the electrons and the holes. Some nitrides such as Ta_3N_5 [3−5] were also reported as photocatalysts under visible light, but not all of them were stable under irradiation. On the other hand, the orbitals of transition elements in multimetal oxide could hybridize the primal orbitals to narrow the band gap. In this case, Zou et al. found that $InNbO_4$ and $InTaO_4$ could evolve H_2 from pure water under visible light irradiation.[7−10]

To explore an approach to develop the novel visible light corresponding to photocatalysts more efficiently, one of the photocatalyst material design methods, which combines the first-principles energy band calculation with the crystal structure analysis, has been successfully developed in this paper.

The electronic structures of some multi-metal oxides which consist of Ag, such as $AgInW_2O_8$,[11] $AgTaO_3$,[2] and $AgNbO_3$,[12] have been studied. Their valence bands (VB) are all constructed by the hybridized Ag-4d orbitals and O-2p orbitals, and their conduction bands (CB) are constructed by the hybridized Ag-5s orbitals and other orbitals, such as In-5s orbitals and W-5d orbitals (in $AgInW_2O_8$), Ta-5d orbitals (in $AgTaO_3$), and Nb-4d orbitals (in $AgNbO_3$). But in these studies, the individual contribution of Ag to the valence band and the conduction band has not been investigated clearly. To study the individual contribution of Ag to the valence band and the conduction band, Ag and the element Al, which only has 3s and 3p orbitals but does not have d orbitals, were selected in our study. $AgAlO_2$ has two typical structures, the hexagonal structure and the orthorhombic structure. But the orthorhombic structure consists of dense polyhedron layers. This means that such a structure would be more favorable for transferring electron−hole pairs. So the $AgAlO_2$ with the orthorhombic crystal structure of space group $Pna2_1$ was chosen to execute the calculation analysis. The energy band, crystal, and electronic structures of $AgAlO_2$ were discussed in detail. Then, the sample was prepared and the photocatalytic AR decomposition over the photocatalyst under visible light irradiation was investigated to test the validity of the material design method.

II. Computational and Experimental Methods

Material Design Details. As mentioned above, in the studies of $AgInW_2O_8$,[11] $AgTaO_3$,[12] and $AgNbO_3$,[12] the individual contribution of Ag to the valence band and the conduction band has not been investigated clearly. To achieve the intention, a suitable material should be dissectionally chosen. Ag_2O seems to be the most adequate candidate, but the band gap of Ag_2O is too narrow to be a photocatalyst. The band gap breadths of silver oxides are influenced nearly by the bond length of Ag−O. In Table 1, the bond lengths of Ag−O in the familiar Ag_2O are smaller than 2.17 Å, and the bond length of Ag−O in $AgTaO_3$, which has high photocatalytic activity under ultraviolet light,

* Author to whom correspondence should be addressed. E-mail: zgzou@nju.edu.cn.
‡ Department of Materials Science and Engineering, Nanjing University.
§ National Laboratory of Solid State Microstructures, Nanjing University.
† Ecomaterials Center, National Institute for Materials Science.
⊥ Ecomaterials and Renewable Energy Research Center, Nanjing University.

10.1021/jp055924t CCC: $33.50
Published on Web 05/27/2006

TABLE 1: The Ag−O Bond Length of Ag_2O, $AgTaO_3$, and $AgAlO_2$

	space group	Ag−O bond length/Å	av Ag−O bond length /Å
Ag_2O	$P\bar{3}m1$[13]	2.161, 2.161, 2.161	2.161
	$Pn\bar{3}mS$[14]	2.061, 2.061	2.061
	$Pn\bar{3}mZ$[15]	2.048, 2.048	2.048
$AgTaO_3$	$R\bar{3}cH$[16]	2.462, 2.462, 2.462	2.462
$AgAlO_2$	$Pna2_1$[17]	2.348, 2.360, 2.412, 2.477	2.399

is 2.46 Å. $AgAlO_2$, which is researched here, matches the condition that the bond length of Ag−O is between 2.17 and 2.46 Å; at the same time, the choice of the element Al could meet the intention of this study.

Calculations. The lattice parameters of the $AgAlO_2$ model were optimized, and then the optimized $AgAlO_2$ model was calculated and the ground-state energy band by using the standard CASTEP package.[18] The lattice parameters and coordinates of the atoms in $AgAlO_2$ are listed in the Table 2. The CASTEP code is a plane-wave pseudopotential total energy calculation method that is based on the density functional theory (DFT). In our calculational study, the electronic wave functions were expanded in a plane-wave basis set up to a 340 eV cutoff. The FFT grid of the basis was $30 \times 40 \times 30$. And the self-consistent field (SCF) tolerance was 1×10^{-6} eV/atom. The ultrasoft pseudopotential and $5 \times 4 \times 5$ k-point for sample were chosen in the calculation. The electronic exchange-correlation energy was treated within the framework of the generalized gradient approximation (GGA), which was superior to the local density approximation (LDA). The calculations of the energy band and density of states (DOS) were both executed.

Experiments. Cation exchange reaction was used to prepare the polycrystalline $AgAlO_2$.[17] The precursor $LiAlO_2$ was first prepared by reaction of Al_2O_3 (99.0%) with a stoichiometric amount of Li_2CO_3 (99.99%) at 750 °C for 12 h, and then reground. The mixed powder was sintered at 1000 °C for 12 h and the white $LiAlO_2$ powder was obtained. The powder was mixed with $AgNO_3$ (99.8%) and KNO_3 (99.0%) at a molar ratio of 1:2:2 in an agate mortar. Then the mixture was heated in air at 275 °C for 12 h. The resulting sheet sample that was washed by distilled water became powder. At last, the sample was dried in air at room temperature.

The crystal structure of the powder sample was determined by the X-ray diffraction method (Rigaku Denki, D/MAX-RA, Japan) with Cu Kα_1 radiation. Intensity data were collected from 15° to 75° in 2θ at room temperature; the scan speed was 10 deg min^{-1}, and the scan step was 0.02°. The diffuse reflectance spectra of the sample were analyzed with a UV−visible spectrometer (UV-2401, Shimadzu, Japan). The surface area was determined by BET measurement (TriStar-3000, Micromeritics, America).

The photocatalytic reaction system consisted of a 300 W Xe arc lamp, cutoff filter, and a water cooler trough (preventing the thermal catalytic effect) that was used to locate the reaction cell. The photocatalytic decomposition of AR was carried out with 0.3 g of $AgAlO_2$ powder suspended in 100 mL of AR solution in a Pyrex glass cell under 2 h of irradiation. Before irradiation the suspensions were magnetically stirred in the dark for several hours to ensure establishment of an adsorption/desorption equilibrium of dye on the sample surface. The AR solution concentration was about 16 mg/L and the pH value of the solution was nearly 7.5 after the dye reached the adsorption/desorption equilibrium on the sample surface. The whole photocatalytic reaction was conducted in air at about 30 °C (the temperature of the reaction solution). The suspension samples including the photocatalyst and AR solution were separated by the centrifuge, and the solution samples were analyzed by the UV−visible spectrometer (CARY 50 Probe, Varian, America) and the total organic carbon (TOC) measurer (TOC-5000, Shimadzu, Japan). The AR decomposition rate was calculated as below: at the irradiation time of t min (including the irradiation times 0, 20, 40, 60, 80, 100 and 120 min), the solution samples (a certain volume, about 2 mL) after centrifugal treatment were pH adjusted with an ammonia solution drip (pH 12) and the UV−visible absorbance spectra were measured, and their UV−visible absorbance spectra all presented a characteristic peak at 486 nm, because the absorbance value of the 0 min solution sample was A_0, and the absorbance value of the t min solution sample was A_t, so at the time of t min, the AR decomposition rate $DR(t) = (A_0 - A_t)/A_0 \times 100\%$.

The photocatalytic decomposition of acetaldehyde was carried out with 0.3 g of the powdered photocatalyst. The photocatalyst was placed at the bottom of a Pyrex glass cell. The reaction was in a gas-closed system with a gas-circulated pump. The optical system for the catalytic reaction included a 300 W Xe arc lamp (focused through a shutter window), a cutoff filter (providing visible light of different wavelengths), and a water filter (to prevent IR irradiation). The concentration of the CH_3CHO gas mixture was 1270 and 680 ppm with nonfilter and $\lambda \geq 420$ nm filter, respectively. The concentrations of CO_2 and acetaldehyde were detected by the gas chromatograph (GC-14B with FID detector, Shimadzu). The yield of CO_2 was calculated for the mineralization rate of the CH_3CHO.

III. Results and Discussion

Crystal Structure and Energy Band. The calculating $AgAlO_2$ model was an orthorhombic crystal structure with space group $Pna2_1$. Figure 1a represents a unit cell of $AgAlO_2$ and Figure 1b shows the polyhedron model of $AgAlO_2$. Corresponding to Figure 1a, Table 3 lists the bond lengths and bond angles in the $AgAlO_2$ crystal. Ag, Al, and O atoms in $AgAlO_2$ all occupy Wyckoff position 4a. The $AgAlO_2$ crystal consists of two kinds of tetrahedra, AgO_4 and AlO_4. In the XY-plane, the AgO_4 or AlO_4 tetrahedra connects to each other to form zigzag chains by sharing vertexes. Then the chains of AgO_4 and the

TABLE 2: The Lattice Parameters and Coordinates of the Atoms in $AgAlO_2$, Which Is an Orthorhombic Crystal Structure with Space Group $Pna2_1$

		Arris	exptl data			calcd data		
lattice parameters		a (Å)	5.4306			5.2728		
		b (Å)	6.9802			6.7628		
		c (Å)	5.3751			5.3626		
	atom	Wyckoff site	x	y	z	x	y	z
atomic coordinates	Ag	4a	0.0532	0.6268	0.9969	0.0598	0.6427	1.0069
	Al	4a	0.0610	0.1251	0.0000	0.0706	0.1239	−0.0013
	O1	4a	0.0311	0.0723	0.3209	0.0342	0.0679	0.3119
	O2	4a	0.1283	0.6765	0.4345	0.1117	0.6681	0.4346

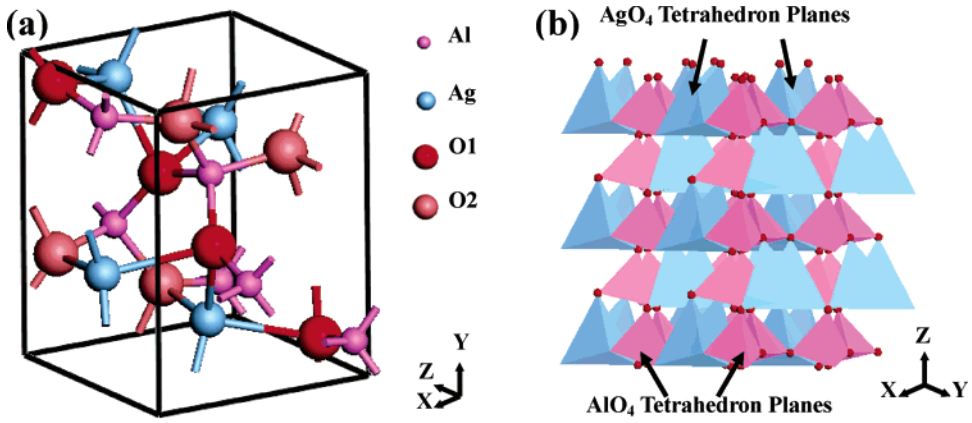

Figure 1. The crystal structure of $AgAlO_2$ with orthorhombic structure: (a) the ball-and-stick model—it is obvious that every Al atom connect with two O1 atoms and two O2 atoms, and each Ag atom also link to two O1 atoms and O2 atoms, so the O1 atoms or the O2 atoms are the juncture of the metal atoms Al and Ag; (b) the polyhedron model—the $AgAlO_2$ crystal consists of two kinds of tetrahedron, AgO_4 and AlO_4. The AgO_4 and AlO_4 tetrahedron connects to each other to form a 3D net structure by sharing vertexes.

TABLE 3: The Bond Lengths and Bond Angles of $AgAlO_2$

	type	value
bond lengths, Å	Ag−O	2.348, 2.360, 2.412, 2.477
	Al−O	1.754, 1.760, 1.761, 1.771
bond angles, deg	O1−Ag−O2	100.9, 103.9, 107.3, 131.6
	O1−Ag−O1	99.3
	O2−Ag−O2	109.8
	O1−Al−O2	107.7, 108.9, 109.0, 110.0
	O1−Al−O1	110.2
	O2−Al−O2	111.1
	Ag−O1−Ag	83.5
	Ag−O2−Ag	86.5
	Al−O1−Al	136.4
	Al−O2−Al	132.9
	Ag−O1−Al	99.9, 103.0, 104.9, 115.2
	Ag−O2−Al	100.9, 102.1, 109.1, 115.7

chains of AlO_4 alternately link by sharing vertexes to form a layer. Layers join each other also by vertexes to construct the three-dimensional network.

The calculated energy band is shown in Figure 2a. The Fermi energy, defined as the highest occupied energy level, has been taken as the valence band maximum (VBM). The VBM is located at the boundary of the Brillouin zone, U point. And the conduction band minimum (CBM) is situated at the middle of the Brillouin zone, Γ point. This means that $AgAlO_2$ is an indirect-gap semiconductor material. A minimum band gap between VBM and CBM is about 1.1(6) eV, which it means that $AgAlO_2$ has the ability to respond to the visible light.

Figure 2b shows the total density of states (TDOS) and partial density of states (PDOS), corresponding to the energy region in Figure 2a. Table 4 presents the projected weights of wave functions at the valence band top and the conduction band bottom. It is clear that the valence band top mainly consists of O-2p orbitals and Ag-4d orbitals, where Ag-4d5s5p, and Al-3s3p orbitals hybridize with O-2p. The DOS peaks at the top of the valence band are constructed of both O-2p and Ag-4d orbitals, and the contribution of Ag-5s5p and Al-3s3p orbitals is negligibly small. The conduction band bottom is mainly constructed of the Ag-5s5p orbitals, and the contribution of the Al and O electronic orbitals is small. These means that $AgAlO_2$ is a suitable material to be selected to investigate the individual contribution of Ag to the valence band and the conduction band.

Photophysical and Photocatalytic Properties. The XRD spectra show that our sample is $AgAlO_2$ of space group $Pna2_1$ (in Figure 3), because the indexed result is in good agreement with that reported in the JCPDS database card No. 21-1070, except for some small peaks of Ag and $LiAlO_2$ impurity, but the metal Ag cannot exhibit photocatalysis, and the $LiAlO_2$ that was the precursor of $AgAlO_2$ is not able to absorb light with a wavelength larger than 290 nm, so the impurity of Ag and $LiAlO_2$ did not influence the characterization of photocatalytic experiments of $AgAlO_2$ in our experimental conditions. According to the diffuse reflectance spectra of the sample (in Figure 5), the band gap is estimated at about 2.8(1) eV, which is larger than the calculated value. The reasons are as follows: on one hand, because the discontinuity in the exchange-correlation potential is not taken into account within the framework of density functional theory (DFT), theoretical values of the energy gap between unoccupied and occupied orbitals in semiconductors and insulators are underestimated compared with experimental ones;[19] on the other hand, it is considered that the optical band gap does not originate from bulk, but from surface and defects.[20,21]

Zhao et al. have studied the photooxidation mechanism of dye AR with TiO_2 as photocatalyst.[22] In our experiment the photocatalytic activity of $AgAlO_2$ was characterized by the experiment of photocatalytically decomposing the dye AR. The results are shown in Figure 4. When the suspensions were magnetically stirred in the dark for several hours to ensure establishment of an adsorption/desorption equilibrium of dye on the sample surface, the AR solution concentration decreased only a little because of the adsorption, but after the Xe lamp was turned on, the AR solution concentration decreased rapidly, especially in the first 20 min, where the concentration decreased about 42%, which means that this reaction is a light-responding reaction. The AR solution decomposed about 70% after 2 h of irradiation with visible light. It was found that the self-photolysis decomposition rate of AR solution was about 25% in 2 h in the same conditions. The measurement of TOC reveals the average mineralization rate is 24.4% after 2 h of visible light irradiation. The band gap of $AgAlO_2$ is 2.8(1) eV, which means that $AgAlO_2$ could show photoabsorption in the visible light region ($\lambda \geq 420$ nm), but the photoabsorption is weak. In the catalytic reaction, the surface area is an important factor for the catalytic activity. The surface area of the $AgAlO_2$ sample is only 3.9 m^2/g. Since an efficient photocatalytic reaction process occurs on the photocatalyst surface, the smaller surface area of $AgAlO_2$ might lead to the decrease of the effective photocatalytic reaction. The study of the effects of surface area on the effective photocatalytic reaction is in progress, which is believed to further help in understanding the new photocatalysts.

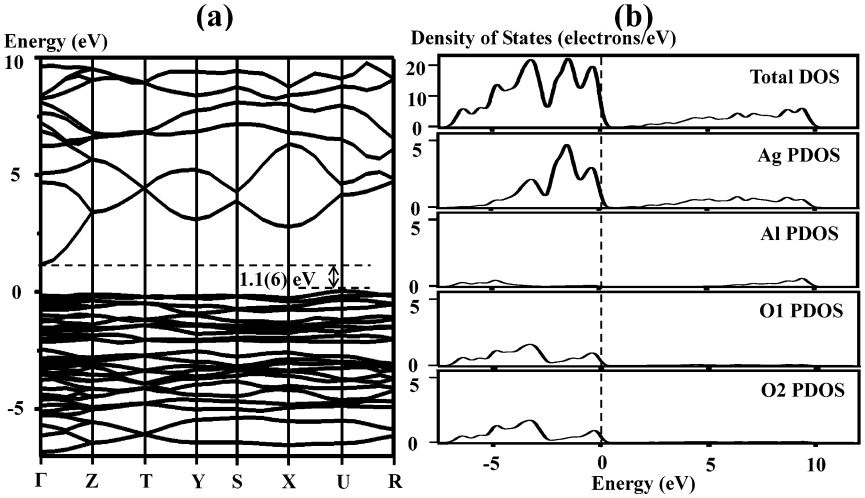

Figure 2. The calculated energy band and density of states (DOS) of $AgAlO_2$: (a) the energy band—the $AgAlO_2$ crystal is an indirect band gap semiconductor and its $E_g = 1.1(6)$ eV; (b) the density of states—the valence band top mainly consists of the hybridized Ag-4d orbitals and O-2p orbitals, while the conduction band bottom is mainly constructed of the Ag-5s5p orbitals.

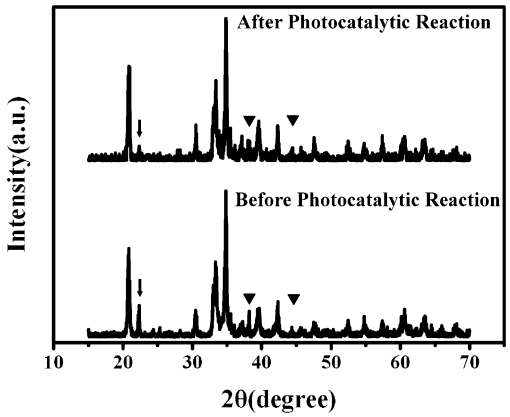

Figure 3. The XRD patterns of $AgAlO_2$, and (▼) Ag and (↓) $LiAlO_2$ peaks.

TABLE 4: Projected Weights of Wave Functions at the Valence Band and the Conduction Band

elements	orbitals	VB, %	CB, %
Ag	5s	2	22
	5p	2	42
	4d	45	2
Al	3s	1	2
	3p	2	16
O1	2s	0	1
	2p	24	7
O2	2s	0	1
	2p	24	7

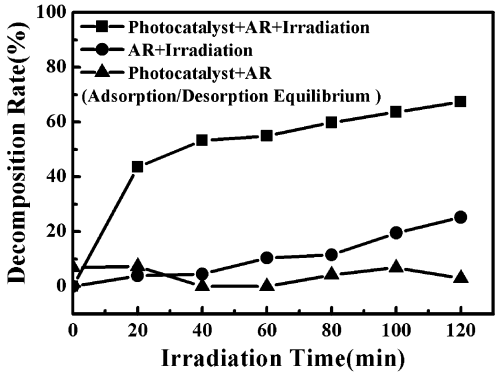

Figure 4. AR decomposition over the $AgAlO_2$ sample was performed under visible light ($\lambda > 420$ nm) at room temperature (ca. 30 °C) in air [the powdered photocatalyst, 0.3 g; the AR solution, 16 mg/L, 100 mL (pH ~7.5)]. The AR solution decomposed about 70% after 2 h of irradiation with visible light, and the photocatalytic efficiency of $AgAlO_2$ was about three times the self-photolysis efficiency (the self-photolysis decomposition rate of AR solution was about 25% in 2 h in the same conditions).

The wavelength dependence of the photocatalytic activity of a semiconductor is often used to distinguish if the reaction is really driven by light. In our experiment, the light wavelength dependence of the AR decomposition rate was observed from $\lambda \geq 350$ nm (full arc of the Xe lamp, without filter) to $\lambda \geq 500$ nm with different cutoff filters (in Figure 5). If a reaction is driven by light, the variation of the light wavelength will directly affect the number of photons entering the reaction system and then the photocatalytic properties. In the present work, it is obvious that the variation of the photocatalytic properties over $AgAlO_2$ was closely relevant to the light wavelength, suggesting that the AR catalytic degradation over $AgAlO_2$ was truly driven by light. And when the 500 nm cutoff filter was used, there was the same decreased concentration of the AR solution (about 10%) with and without the $AgAlO_2$ photocatalyst, whcih means the decrease of concentration of the AR might result from self-photolysis decomposition. The light was irradiated through the suspension, but the reaction did not begin, which means the reaction is not a photochemical reaction. After the photocatalytic reaction, the $AgAlO_2$ sample was analyzed by XRD again. The XRD spectra showed that the sample remained $AgAlO_2$ of space group $Pna2_1$ and also included the Ag and $LiAlO_2$ impurity (in Figure 3). It is known that the photooxidation/photodissolution of catalyst might occur on the photocatalyst surface in the photocatalytic reaction. The samples before and after reaction were analyzed by XPS. There was no shift for the peaks of Ag-3d and Al-2p in the surface of samples before and after reaction. This suggests that the surface of $AgAlO_2$ is stable in the photocatytic reaction, which means that the sample was stable in the photocatalytic reaction. The above proves the reaction of AR decomposition was photocatalysis.

In our photocatalytic experiments, the contrast experiment of the photocatalytic decomposing AR on TiO_2 was not executed, because $AgAlO_2$ could not exhibit photocatalytic activity at the irradiation light wavelength of $\lambda \geq 500$ nm (this cutoff wavelength is only a little larger than the light absorbable limitation wavelength of $AgAlO_2$, about 50−60 nm), and it could be concluded that the photocatalytic decomposing AR

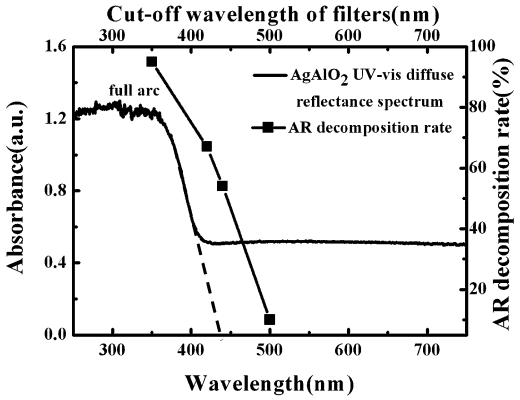

Figure 5. The UV−visible diffuse reflectance spectra of $AgAlO_2$ and the wavelength dependence of the AR decomposition rate with different cutoff filters after light irradiation for 120 min over $AgAlO_2$ at room temperature (ca. 30 °C) in air: when the full arc of the Xe lamp was use as the light source, the photocatalytic decomposition rate reached 95%, and when the 500 nm cutoff filter was used in the photocatalytic experiment, the decomposition rate decreased to about 10% (the value was nearly equal to the self-photolysis decomposition rate in the same conditions).

on $AgAlO_2$ was an intrinsic photocatalytic reaction but not a dye-assisted photocatalytic mechanism, but the photocatalytic decomposing of AR over TiO_2 was a dye-assisted photocatalytic reaction.[22] Because of the dye-assisted photocatalytic mechanism, assisted by the different dyes, the photocatalysts could exhibit photocatalytic activity at the cutoff wavelength much more than at their light absorbable limitation wavelength, even more than 200 nm, such as $CaIn_2O_4$.[23]

It was also observed that the $AgAlO_2$ photocatalyst is effective in the gas-medium photocatalytic reaction under 300 W Xe arc lamp irradiation and visible light irradiation ($\lambda \geq 420$ nm). The results of the acetaldehyde photocatalytic decomposition are showed in Figure 6.

Discussion. First, for the past several decades, research on the photocatalysis surrounded several elements, such as Ti, Ta, Nb, V, W, Mo, In, Ga, and Bi, but $AgAlO_2$ does not include these elements. Second, the multimetal oxide materials which could photocatalytically decomposed organic contaminations with high activity are listed here: (1) Bi_2WO_6,[24] $BiVO_4$,[25] $PbBi_2Nb_2O_9$, [26] and $ZnBi_{12}O_{20}$[27]—and in these photocatalysts, the valence bands mainly consist of hybridized s orbitals, p orbitals, and d orbitals, and the conduction bands are mainly constructed by s orbitals, p orbitals, or hybridized s orbitals and p orbitals; (2) in the photocatalyst $CaBi_2O_4$,[28] the valence band mainly consists of hybridized Bi-6s orbitals and O-2p orbitals, and the conduction band is mainly constructed of Bi-6p orbitals; (3) in $CaIn_2O_4$,[23] the valence band consists of O-2p orbitals, and the conduction band is constructed of In-5s orbitals. But the band structure of $AgAlO_2$ is different from any mentioned above. Therefore, though $AgAlO_2$ does not exhibit as high activity as the materials mentioned above, special element composition and band structure make $AgAlO_2$ a novel photocatalyst. And such band structure supplies some different ideas for developing new photocatalysts.

For the photocatalyst $AgAlO_2$, the valence band top mainly consists of O-2p orbitals and Ag-4d orbitals. This seems that the mobility of holes generated by band-gap excitation is expected to be high, because the holes could be excited from the hybridized Ag-4d orbitals and O-2p orbitals, so the electronic structure of the valence band top is more preferable for photocatalysis than the $InTaO_4$, which consists of a valence band top of only O-2p orbitals.[29] But the energy band in Figure 2a shows the valence band is very flat. The relativity of E and υ is know clearly $\upsilon = \nabla_k E(k)/\hbar$, where E is the energy of the electron and υ is the velocity of the electron. If $\nabla_k E(k)$ is small (band is flat), υ is also small. So, the valence band being flat means that holes are easily localized round Ag or O or move very slowly, though they could be transferred along O−Ag−O chains. This implies that the contribution of holes to photocatalysis is very limited. However, in contrast to the valence band, the conduction band is mainly constructed of Ag-5s5p orbitals, and the conduction band is very abrupt, suggesting that the mobility of the electrons was strong. Therefore, to a certain extent, such a condition is a possible advantage for restraining recombination of the charge carriers.

The crystal structure influences the energy band and electronic structures. And another essential of the crystal structure, which was usually neglected, is that the crystal structure impacts the move efficiency of the charge carriers. The $AgAlO_2$ structure has been introduced above, and the detailed crystal structure will be discussed below. According to calculation results, the AgO_4 tetrahedron planes perform the main transmission job of the charge carriers, and the contribution of the AlO_4 tetrahedron planes is negligibly small. So the bond angles of Ag−O−Ag and O−Ag−O are regarded here. In the $AgAlO_2$ structure, the bond angles of O−Ag−O and Ag−O−Ag range from 99.3° to 131.6° and from 83.5° to 86.5°, respectively (in Table 3). But because of the high symmetry, in the perovskite structure, the bond angles of O−metal−O and metal−O−metal are all about 180°. This means the charge carriers could move to the sample surface through fewer atoms in the perovskite structure than in

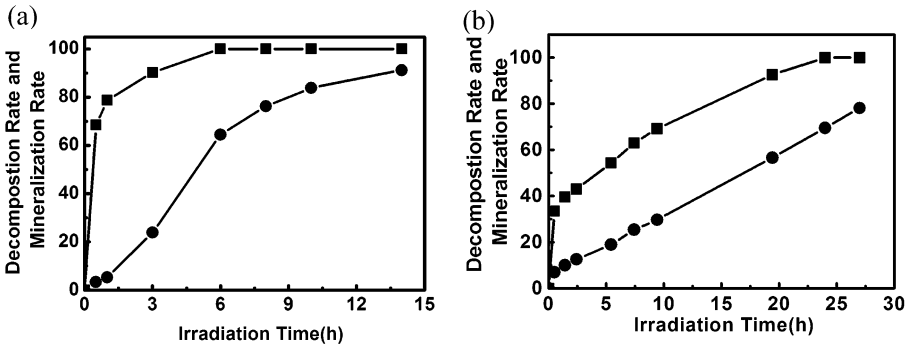

Figure 6. CH_3CHO photocatalytic decomposition over $AgAlO_2$ under ultraviolet + visible light (a) and visible light (b). (a) Reaction conditions: 300 W Xe lamp, full arc; catalyst, 0.3 g; a gas-closed system with a gas-circulated pump; initial concentration of CH_3CHO about 1270 ppm. (■) The decomposition rate of CH_3CHO, (●) the mineralization rate of CH_3CHO; (b) Reaction conditions: 300 W Xe lamp, $\lambda \geq 420$ nm; catalyst, 0.3 g; a gas-closed system with a gas-circulated pump; initial concentration of CH_3CHO, about 680 ppm. (■) The decomposition rate of CH_3CHO, (●) the mineralization rate of CH_3CHO.

the $AgAlO_2$ structure. From the crystal structure viewpoint, the more ideal model for the most effective transfer of the charge carriers is mentioned below: in a crystal that is constructed of MO_6 octahedral layers, these octahedra should be equilateral polyhedra and connect each other by sharing vertexes, at the same time the metal−O−metal and O−metal−O angles are nearly 180° (this means that the crystal structure has high symmetry, which usually belongs to a cubic or tetragonal system), such as $SrTiO_3$;[30,31] in a crystal that is composed of MO_4 tetrahedral layers, these tetrahedra should be freakish polyhedra to augment bond angles and connect each other by sharing vertexes, at the same time the metal−O−metal and O−metal−O angles are nearly 180° (this implies that the crystal structure has lower symmetry, which usually belongs to a triclinic or monoclinic system); but as to the crystals which have general symmetry, the crystal structure that consist of both MO_6 octahedra and MO_4 tetrahedra should be more favorable, such as $InVO_4$.[9]

Now the projected weights of wave functions at the valence band and the conduction band and the detailed crystal structure in $AgAlO_2$ have been analyzed intensively. To further develop the Ag-system multimetal oxides, Al should be exchanged for the element, which could improve the existing electronic structure and crystal structure in $AgAlO_2$. A series of new Ag-system multimetal oxides have been investigated, and their properties will be reported somewhere.

IV. Conclusions

The energy band, crystal, and electronic structures of $AgAlO_2$ were investigated intensively. The calculated results demonstrated that $AgAlO_2$ is a suitable material to be selected to investigate the individual contribution of Ag to the valence band and the conduction band. As an indirect band gap semiconductor, the calculated indirect band gap $E_g = 1.1(6)$ eV and the experimental estimated band gap was 2.8(1) eV. The photocatalytic activity of $AgAlO_2$ was characterized by photocatalytic decomposing AR under visible light irradiation. The advantages and disadvantages of the $AgAlO_2$ crystal and electronic structures were also analyzed. It will be useful to carry out further research in developing the new Ag-system multimetal oxides. It was shown that the energy band analysis combining with the crystal structure analysis is a feasible approach to develop new photocatalysts which could exhibit photocatalytic activity under visible light.

Acknowledgment. The generous financial support of this work from the National Natural Science Foundation of China (Nos. 20373025 and 50472067) is gratefully acknowledged.

References and Notes

(1) Honda, K.; Fujishima, A. *Nature* **1972**, *238*, 37.
(2) Asahi, R.; Morikawa, T.; Ohwaki, T.; et al. *Science* **2001**, *293*, 269.
(3) Domen, K.; Hara, M.; Kondo, J. N.; Tanaka, T. *Bull. Chem. Soc. Jpn* **2000**, *73*, 1307.
(4) Hara, M.; Chiba, E.; Ishikawa, A.; et al. *J. Phys. Chem. B* **2003**, *107*, 13441.
(5) Hara, M.; Hitoki, G.; Takata, T.; et al. *Catal. Today* **2003**, *78*, 555.
(6) Hara, M.; Takata, T.; Kondo, J. N.; Domen, K. *Catal. Today* **2004**, *90*, 313.
(7) Zou, Z.; Ye, J.; Arakawa, H. *Chem. Phys. Lett.* **2000**, *332*, 271.
(8) Zou, Z.; Ye, J.; Sayama, K.; Arakawa, H. *Nature* (*London*) **2001**, *414*, 625.
(9) Ye, J.; Zou, Z.; Arakawa, H.; et al. *J. Photochem. Photobiol. A*: *Chem.* **2002**, *148*, 79.
(10) Zou, Z.; Arakawa, H. *J. Photochem. Photobiol. A*: *Chem.* **2003**, *158*, 145.
(11) Tang, J.; Zou, Z.; Ye, J. *J. Phys. Chem. B* **2003**, *107*, 14265.
(12) Kato, H.; Kobayashi, H.; Kudo, A. *J. Phys. Chem. B* **2002**, *106*, 12441.
(13) Kabalkina, S. S.; Popova, S. V.; Serebrjanaja, N. R.; et al. *Dokl. Akad. Nauk SSSR* **1963**, *152*, 853.
(14) Wyckoff, R. W. G. *Am. J. Sci.* **1921**−**1938**, *Ser. 5*, 1; **1922**, *Ser. 3*, 184.
(15) Norby, P.; Dinnebier, R. E.; Fitch, A. N. *Inorg. Chem.* **2002**, *41* (14), 3628.
(16) Wolcyrz, M.; Lukaszewski, M. *Z. Kristallogr.* **1986**, *177*, 53.
(17) Li, J.; Sleight, A. W. *J. Solid State Chem.* **2004**, *177*, 889.
(18) Segall, M. D.; Lindan, P. L. D.; Probert, M. J.; et al. *J. Phys.*: *Condens. Matter* **2002**, *14*, 2717.
(19) Hohenberg, P.; Kohn, W. *Phys. Rev. B* **1964**, *136*, 864−871.
(20) Hedin, L.; Lundqvist, S. *Solid State Phys.* **1969**, *23*, 1.
(21) Hybertsen, M. S.; Louie, S. G. *Phys. Rev. B* **1986**, *34*, 5390.
(22) Liu, G.; Li, X.; Zhao, J. *J. Mol. Catal. A*: *Chem.* **2000**, *153*, 221.
(23) Tang, J.; Zou, Z.; Ye, J. *Chem. Mater.* **2004**, *16*, 1644.
(24) Kudo, A.; Hijii, S. *Chem. Lett.* **1999**, *10*, 1103.
(25) Kudo, A.; Ueda, K.; Kato, H.; et al. *Catal. Lett.* **1998**, *53* (3−4), 229.
(26) Kim, H. G.; Hwang, D. W.; Lee, J. S. *J. Am. Chem. Soc.* **2004**, *126*, 8912.
(27) Tang, J.; Ye, J. *Chem. Phys. Lett.* **2005**, *410*, 104.
(28) Tang, J.; Zou, Z.; Ye, J. *Angew. Chem., Int. Ed.* **2004**, *43*, 4463.
(29) Matsushima, S.; Obata, K.; Nakamura, H.; et al. *J. Phys. Chem. Solid* **2003**, *64*, 2417.
(30) Hutton, J.; Nelmes, R. J. *J. Phys. C* **1981**, *14*, 1713.
(31) Domen, K.; Nalto, S.; Onlshl, T.; et al. *J. Phys. Chem.* **1982**, *86*, 3657.